Article:
Ghadbeigi, H., Pinna, C. orcid.org/0000-0002-9079-1381 and Celotto, S. (2013) Failure mechanisms in DP600 steel: Initiation, evolution and fracture. Materials Science and Engineering: A, 588. pp. 420-431. ISSN 0921-5093

https://doi.org/10.1016/j.msea.2013.09.048

Failure mechanisms in DP600 steel: initiation, evolution and fracture

H. Ghadbeigi[a*], C, Pinna[a], S. Celotto[b]
[a] The University of Sheffield, Department of Mechanical Engineering, Mappin Street, Sheffield, S1 3JD, UK
[b] Tata Steel R&D, IJmuiden, 1970 CA, The Netherland
[*]Corresponding author: h.ghadbeigi@shef.ac.uk , Tel: 0044 (0) 114 222 73862, Fax: 0044 (0) 114 222 7890

Abstract
Local deformation and damage mechanisms have been studied for a commercial DP600 steel using in-situ tensile testing inside a scanning electron microscope (SEM) in combination with Digital Image Correlation (DIC). Different gauge geometries have been used to study damage evolution processes during tensile testing up to final failure. Strain distributions have been measured within the ferrite and martensite phases, together with the corresponding strain values for identified damage initiation mechanisms. According to the strain maps, large plastic deformation with strain values as large as 4.5 measured within the ferrite phase. Although no failure initiation was observed within the ferrite grains, there was severe deformation localization and slip band formation. The DIC results show that martensite in the studied material is plastically deformable with a heterogeneous strain distribution within the islands with values of up to 0.9 close to the phase boundaries. Failure of the martensite islands occurs mostly due to micro-crack initiation at the boundaries with the ferrite followed by crack propagation towards the centre the islands. As for the ferrite matrix, it is found that its interface with the martensite is strong and cohesive. Localised damage in the matrix occurs by sub-micron void formation within the ferrite adjacent to the interface, as opposed to the separation along the phase boundary itself. A mechanism has been proposed to explain the deformation and damage evolution in the microstructure of the studied DP600 steel up to the final fracture.

Keywords: Dual phase steel, damage evolution, DP600, digital image correlation, martensite deformation

1 Introduction

Dual-Phase (DP) steels are the most common type of Advanced High Strength Steels (AHSS) used in the automotive industry. The combination of high strength and formability imparts improved passenger safety through greater energy absorption capacity and therefore, better crashworthiness. In addition, AHSS has enabled reduced vehicle fuel consumption through weight-reduction by the down gauging of components. The microstructure of DP steels generally consists of a ferrite matrix with embedded martensite islands. The volume fraction and the size of the phases largely determine the tensile strength and formability [1-3]. The multiphase microstructure of DP steels results in a complex micromechanical behaviour. Nevertheless, damage initiation and evolution needs to be understood in order to improve current AHSS and develop new generations of steels.

Several attempts have been made to identify local damage initiation and deformation mechanisms of AHSS. Gerbase et al [4] investigated the mechanisms of damage initiation and final failure behaviour of several DP steels with carbon contents ranging from 0.11-0.12 %wt. They measured the dimensional change of several martensite islands in a DP700 steel

with 15% volume fraction of martensite and reported that this phase undergoes plastic strain values of up to 50% before final fracture. It is found that voids are associated with either non-metallic inclusions or martensite islands in DP steels [5]. The major void formation mechanisms reported [5-7] for DP steels include: 1) decohesion of the ferrite-martensite interface, 2) fracture of martensite islands, and 3) voids generated in the martensite islands due to either the separation of prior austenite grain boundaries between adjacent martensite islands or the localized deformation within the martensite phase. The martensite cracking was found to be more frequent in a coarse martensite microstructure [5, 7]. The martensite failure may occur due to : i) decohesion of prior austenite grain boundaries [8, 9], ii) fracture of martensite islands due to crack initiation [10] and iii) decohesion at the ferrite-martensite interface [11]. These mechanisms have been determined from post-mortem microstructural investigations, therefore the onset of damage initiation has not been accurately identified.

Avramovic-Cingara et al [7] have measured the through thickness strain along the mid-width plane of DP600 samples subjected to uni-axial tensile deformation. They showed that in the martensite, fracture occurs at small strains as low as 0.13. They also reported that the deformation localization starts from the centreline martensite band then propagates towards the neighbouring ferrite regions [11]. However, the localized deformation mechanisms within the martensite islands and their failure mechanisms were not determined as the observations have been made through post-test analyses of the broken specimens. Furthermore, the studied region of the microstructure may not be representative of the bulk material and no analysis is given regarding the strain distribution in the material.

A further study on a DP800 steel [12] revealed new types of voids that initiated due to the failure of ferrite grain boundaries and shear fracture of the ferrite matrix away from the centre of the fracture surface. It is reported that for the ferrite grain boundary voids formed because of deformation mismatch between the grains in the direct neighbourhood of martensite islands. They also found that the fracture of martensite islands was not the most common mechanism in their material.

Even though void initiation mechanisms have been widely studied in DP steels, a comprehensive understanding about local deformation and damage behaviour of such a complex microstructure requires the local deformation to be quantified with respect to the observed mechanisms. The micro-scale deformation of materials has been mainly studied through the observation of microstructural evolution using different techniques including in-situ mechanical testing combined with strain measurements at a microscopic scale [9, 13-17].

Shen et al [13] determined the strain distribution in the ferrite and martensite phases by measuring the average relative elongations of each phase along the tensile direction in various DP steels. They reported that the macroscopic strain at which martensite deformation commenced depended on the microstructural configuration of the steel. This occurs at the early stages of deformation for steels with high martensite volume fractions, while in steels with lower fraction of martensite and higher carbon content martensite deformation starts well after the necking point. Although they measured strain values in the individual phases, no information was given about the damage mechanisms and the associated local strain values in the microstructure.

In recent years the Digital Image Correlation (DIC) technique has been widely used to measure full field displacement and strain distributions over a selected region of specimens

using the natural patterns of microstructures [9, 14]. Ososkov et al [15] measured the local strain partitioning in a DP600 steel during the uniform plastic deformation stage of tensile tests by using both DIC and a microgrid technique. The experiments were carried out in a Scanning Electron microscope (SEM) with the tests interrupted regularly to take images covering an area of about 50µm x 50µm of the microstructure away from the necked region. They also estimated the evolution of local deformation in soft (mainly ferrite) and hard (ferrite and martensite) regions at different locations within the gauge length. They found that the deformation within the martensite-rich regions reached a maximum strain value of 30%, while strain values in the ferrite phase increased continuously to over 70% close to the fracture surface. However, the strain distribution in a given phase was not quantified and local damage mechanisms were not studied.

Kang et al [16] have also used DIC to measure strain partitioning in DP600 steels with different tempering conditions. Although they produced strain maps for the deformed microstructure, the covered area was small relative to the scale of the microstructure. A local true strain value of 0.4 was reported for the initiation of voids between two martensite islands. Consequently, the measured local strain maps could not be related to the already identified damage mechanisms for DP steels [5-7, 12, 18].

In the present research, interrupted in-situ tensile tests have been carried out inside a SEM on specimens with different gauge geometries in order to identify deformation, damage initiation and damage evolution mechanisms in the microstructure of commercial DP600 steel during loading. Digital Image Correlation has been used to measure full field strain maps of the microstructure at different magnifications to study strain evolution within the individual phases in relation to the observed damage initiation mechanisms. A mechanism has been proposed for the full deformation and damage history of the material up to the final fracture.

2 Experiment

Miniature tensile specimens were made from a commercial cold-rolled and annealed DP600 steel strip grade with a thickness of 1.79 mm and a chemical composition of 0.09wt.% C, 1.6wt.% Mn, 0.24wt.% Si, 0.03wt.%Al, 0.04wt.%N and 0.01wt.%P. The material has a classical dual-phase microstructure with 15% martensite volume fraction and a ferrite matrix with a grain size range of 5-20 µm.

The test specimens are shown in Fig. 1 that takes into account the load capacity of the tensile stage. Specimens with the gauge geometry of Fig. 1-a (denoted G1) were used to study the local deformation and damage initiation mechanisms as well as the strain distribution at the scale of the microstructure. The damage evolution mechanisms were investigated using a slightly different gauge geometry (G2) shown in Fig.1-b. The gauge profile of both geometries was machined using electro-discharge wire erosion in order to minimise the local plastic deformation due to the conventional machining processes. For the specimens with the Fig. 1-a geometry, prior to the tensile testing, one of the broad surfaces was mechanically polished and etched in a 2% Nital solution to reveal the microstructure. The tests were then carried out with the loading direction parallel to the rolling direction (RD) according to the procedure developed by the authors in [9] using a 5kN Deben tensile test stage inside the chamber of a CamScan SEM using a crosshead speed of 0.1mm/min. Micrographs of the deforming microstructure were taken at magnifications of 3000X and 9000X. The local deformation within the ferrite and martensite phases was quantified using

Digital Image Correlation(DIC) as explained in [9]. A grid size of 8 x 8 and 16 x 16 pixels were used in DIC analyses for low and high magnifications, respectively.

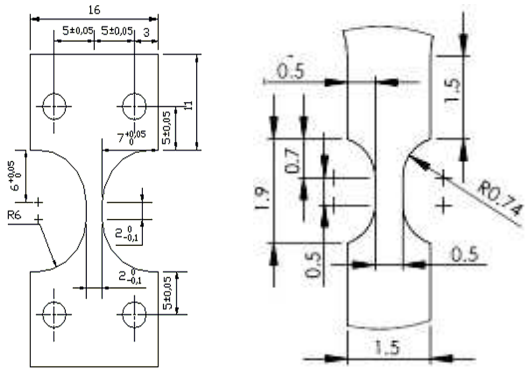

(a)G1 (b)G2

Fig. 1 (a) tensile specimen geometry designed to investigate local deformation and damage initiation mechanisms and (b) the gauge geometry used to study damage evolution mechanisms. All dimensions are in millimetres

Tensile tests using specimens with the gauge geometry of G2 (Fig. 1-b) was used to investigate damage evolution mechanisms. The tests were stopped at different strain levels in the post-uniform elongation stage and close to the final fracture. The specimens were sectioned and metallographically prepared along their mid-width plane. The through thickness strain was calculated using the thickness of the specimens in the centre of the neck measured from the optical micrographs of the mid-width plane. The previously described etching procedure was then used to reveal the microstructure of the specimens at this plane and the deformed microstructure of the material was scrutinized using a high resolution FEG-SEM in order to identify the damage evolution mechanisms at each strain level.

3 Results

3.1 Stress-strain curves

The engineering stress-strain curves have been determined using the load and displacement data measured at the grip section of the G1 and G2 specimens. The curves are plotted in Fig. 2 wherein the solid and broken lines represent the stress-strain data for the specimens with the 2 mm and 0.5 mm gauge lengths, respectively. The intermittent decreases in stress values for the G1 curve are due to the relaxation of the specimen during intervals used to take images for subsequent DIC analysis. It should be noted that the large post uniform elongation is the result of the specimen geometry. The uniform plastic deformation part of the curves is also reduced by the gauge length reduction.

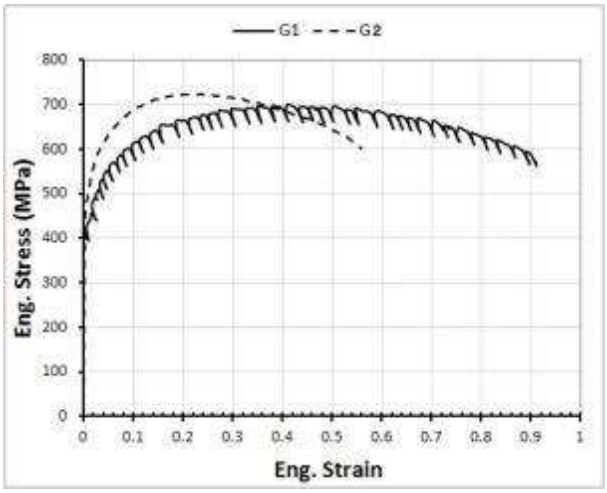

Fig. 2 Engineering stress-strain curves of the material tested with different gauge geometries.

3.2 Deformation and damage initiation mechanisms

Successive micrographs of the deforming microstructure taken during the tests have been analysed to identify the local deformation and damage mechanisms. Fig. 3 shows micrographs of the undeformed (Fig. 3a, c) and deformed microstructure close to the final fracture (Fig. 3b,d) taken at low and high magnifications. It is found that the local deformation commenced with slip bands formation within the largest ferrite grains (F1 and F2 in the figures). The slip bands then appeared in the smaller grains followed by an increase in the density of the bands (F1 in Fig. 3d). The slip bands then crossed into the neighbouring ferrite grains or martensite rich regions to develop localized deformation bands that ran across several grains within the microstructure. The transfer of slip bands across adjacent grains was found to occur at smaller strain levels when the bands are formed in the same direction. It is presumed that this is related to the crystallographic orientation of the grains and therefore, directions of active slip systems.

3.2.1 Deformation and Crack initiation in martensite

The martensite islands can deform in tensile, shear or bending modes according to their configuration with respect to the loading direction and the morphology and deformation state of the surrounding ferrite grains. The failure mechanisms of martensite are discussed in the following sections.

The highlighted areas in Fig. 3 show examples of the different deformation and damage mechanisms observed within the martensite phase. The local displacement of the identified martensite islands with respect to the loading direction indicates that the martensite islands labelled M3 and M6 (Fig.3a) are elongated in the loading direction (that is vertical in the micrographs) whereas a shear deformation is appeared to take place at the vicinity of martensite islands M1 and M5 by the applied local stresses. A combination of bending and tensile deformation was observed for the martensite island M2 as indicated by the arrow. A comparison of the undeformed and deformed microstructures at higher magnification (Fig. 3-c and d) confirms the identified deformation modes. Furthermore, it shows that the phase boundaries maintained their integrity even up to the point where the martensite islands themselves began to fracture where still no decohesion occurred at the interfaces. This is shown in the encircled martensitic region of Fig. 3c where the boundaries of the deformed and undeformed martensite island are compared and the local elongation measured. A total elongation of about 50% is measured up to the point of fracture (Fig.3-d) with no

decohesion at the ferrite -martensite (F-M) interface. However, separation of prior austenite grain boundaries, as a well-known damage mechanism in the martensite phase of DP steels[10] , has been observed as highlighted by the square area in Fig. 3c and d.

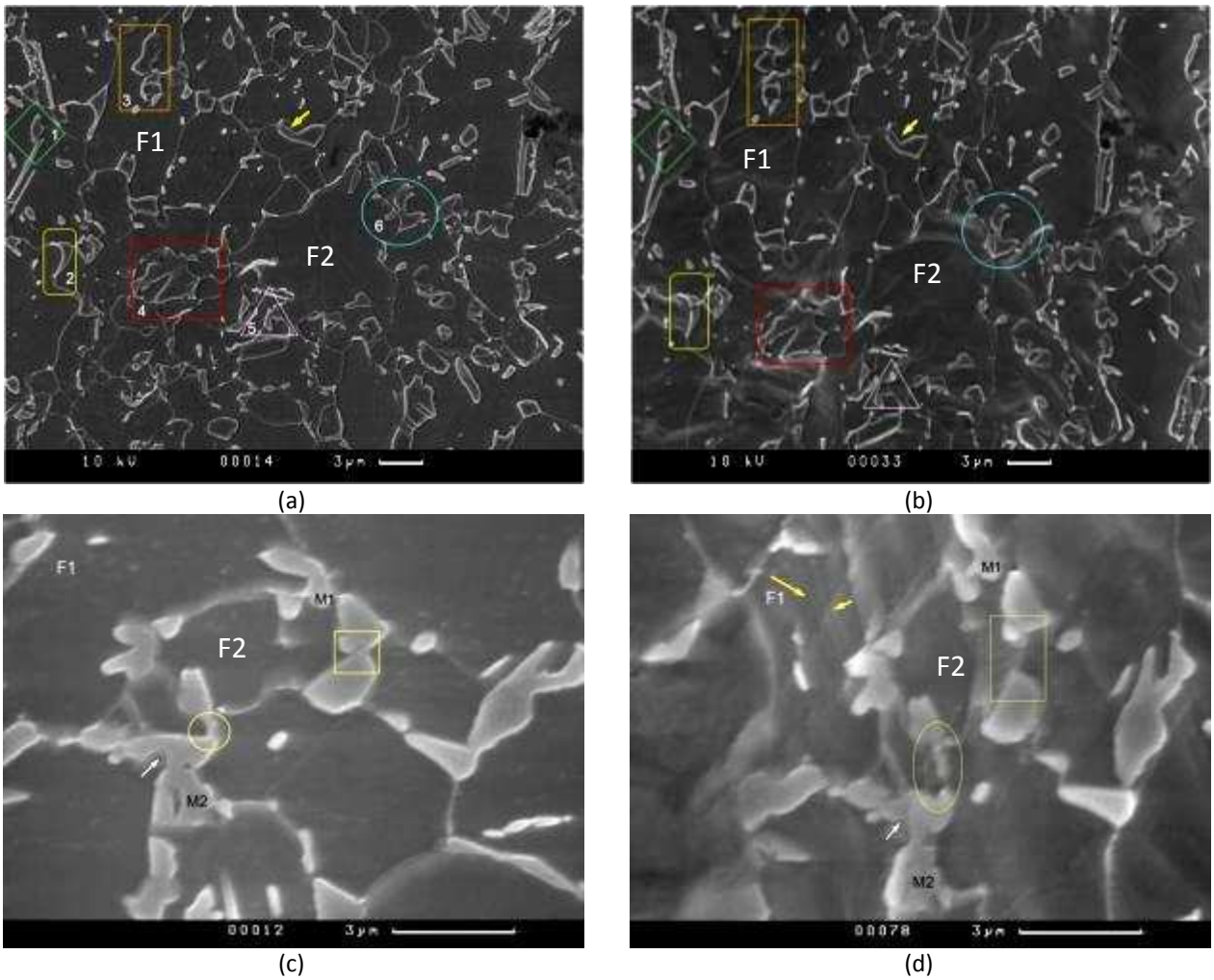

Fig. 3 (a,c) Undeformed and (b,d) deformed microstructure of the specimens after an applied strain of 88% taken at (a,b) 3000X and (c,d) 9000X magnification. The loading direction is vertical in the micrographs. The micrographs show slip bands formation within the ferrite grains prior to the damage of the highlighted martensite islands

Close investigation of the micrographs of the deformed microstructures reveals several of the martensite failure mechanisms in the DP steel studied. Micro-cracks formation in the martensite due to extensive tensile (Fig. 4-a) and bending (Fig. 4-b) deformation is the main local damage initiation mechanism identified. Fig. 4 shows crack initiation and propagation in the martensite phase at several loading steps during the tests. The outline of the undeformed martensite island in Fig. 4 is highlighted and superimposed on the deformed micrographs to show the extent of deformation in that phase.

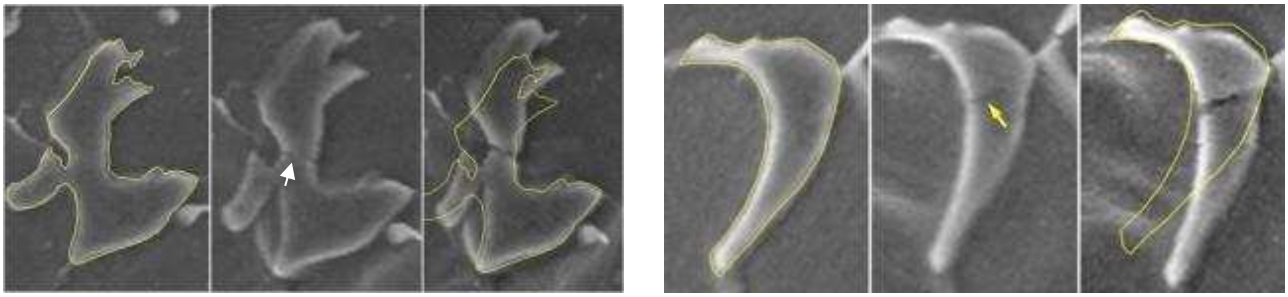

(a) (b)

Fig. 4 (a,c) Undeformed and (b,d) deformed microstructure of the specimens after an applied strain of 88% taken at (a,b) 3000X and (c,d) 9000X magnification.

Fig.4-a shows local necking occurring in the martensite island and microcracks initiating from both sides of the narrow central region indicated by the arrow in the middle image. The cracks grew towards the interior of the martensite island and final fracture occurs at a total elongation of 13.5 % in the martensite island. Fig. 4-b shows that the bending mode imposed on the martensite phase also results in crack initiation from the boundary of the island under tension followed by its propagation towards the centre of the island in a direction that is perpendicular to the local principal loading direction. Martensite fracture occurred as the crack passed through the island. The broken islands then moved rigidly within the microstructure from the plastic deformation of the ferrite phase.

3.2.2 Damage mechanisms at the boundaries

In addition to mechanisms that involve crack initiation and propagation within the martensite islands, failure of the ferrite-martensite (F-M) interface is another damage initiation mechanism that is reported for DP steels [5, 7]. Uggowitzer and Stuwe [19] related this type of failure to the separation of inclusions from the martensite islands close to the interface with ferrite. However, the observations made in the current study like that shown in Fig. 5 revealed that the failure did not occur at the interface itself, instead voids formed within the ferrite phase close to the martensite boundary. Sub-micron voids close to the interface inside the ferrite grains are highlighted by the arrows in Fig. 5a. The voids then elongated through further applied deformation and micro-cracks are formed (Fig. 5b). These then propagate along the interface and martensite islands are separated from the adjacent ferrite grains (Fig. 5c). It should be noted that the crack propagation occurs within the ferrite grain rather than at the interface itself as shown in Fig. 5c and 5d. Fig. 5d shows indeed a martensite island on the fracture surface with some part of the ferrite phase still attached to the island after damage development. It worth noting that, the observed mechanisms are representatives of the microstructural observations in this study. However the statistical analysis of the results is not the subject of the present research.

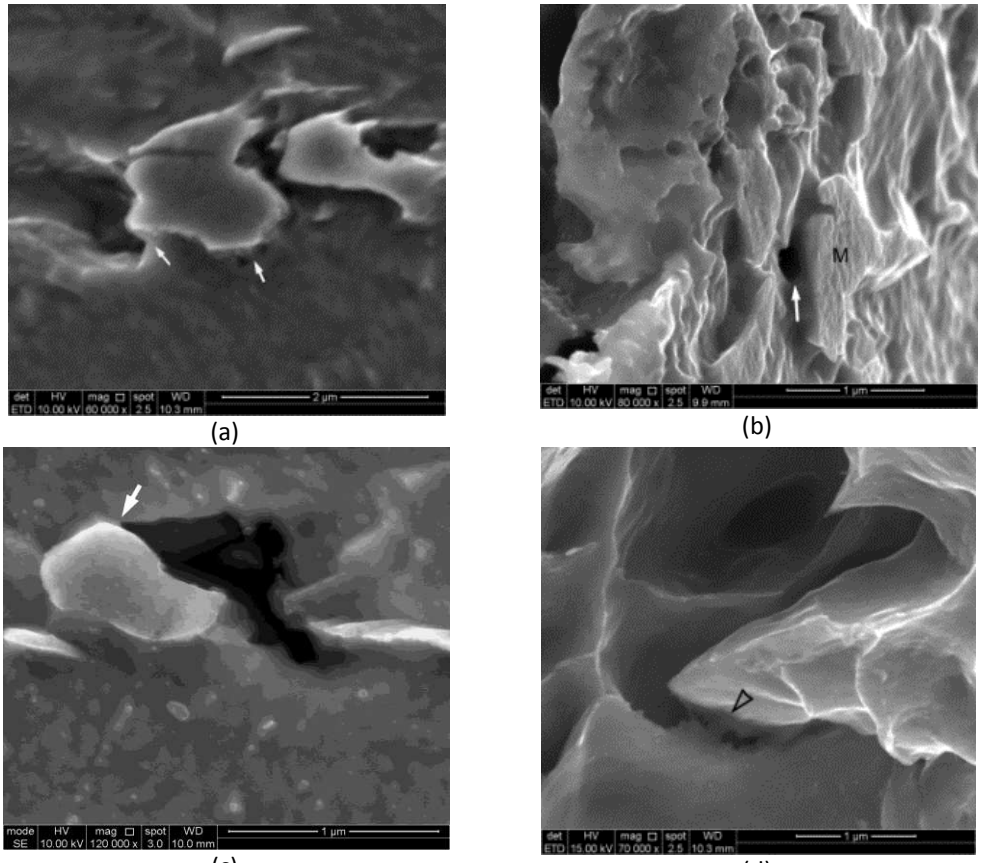

Fig. 5 The damage initiation mechanism at the vicinity of ferrite-martensite interface includes (a) micro-void initiation within the ferrite phase followed by (b) void growth and (c) tearing off the ferrite region along the interface (d) up to the final fracture where some of the ferrite phase attached to the martensite island

A similar behaviour has been identified for the damage initiation at the vicinity of the ferrite grain boundaries. Fig. 6a shows that damage starts by micro-void formation at the triple junction of the ferrite grains and the martensite phase followed by void elongation along the grain boundary. The fact that the generated crack is growing parallel to the loading direction (i.e. horizontal in the micrograph) and cannot cross the grain boundary implies that the grain boundary shows more resistance to the damage process than the bulk phase itself does. This is also shown in Fig. 6b where the ferrite phase on both sides of the grain boundary has failed while the grain boundary has retained its integrity.

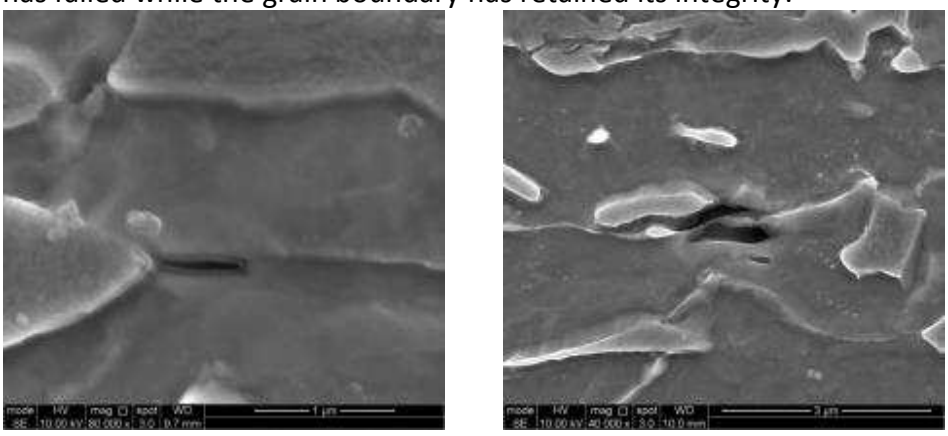

Fig. 6 (a) Void initiation at the triple junction of the grains and (a, b) its growth along the ferrite grain boundary showing that the grain boundary is stronger than the ferrite regions at the vicinity of the boundary

In addition to the identified damage initiation mechanisms at the early stages of the post uniform plastic deformation, sub-micron voids formation is the mechanism that is mostly observed right before the final failure (Fig. 7). Micrographs of Fig. 7a,b show that voids with a size of few hundreds of nano-meters are initiated inside the ferrite phase due to decohesion of fine dispersed carbide particles or Mn-S inclusions from the matrix (Fig. 7c). The latter micrographs show the early stages of voids initiation and coalescence in the ferrite phase.

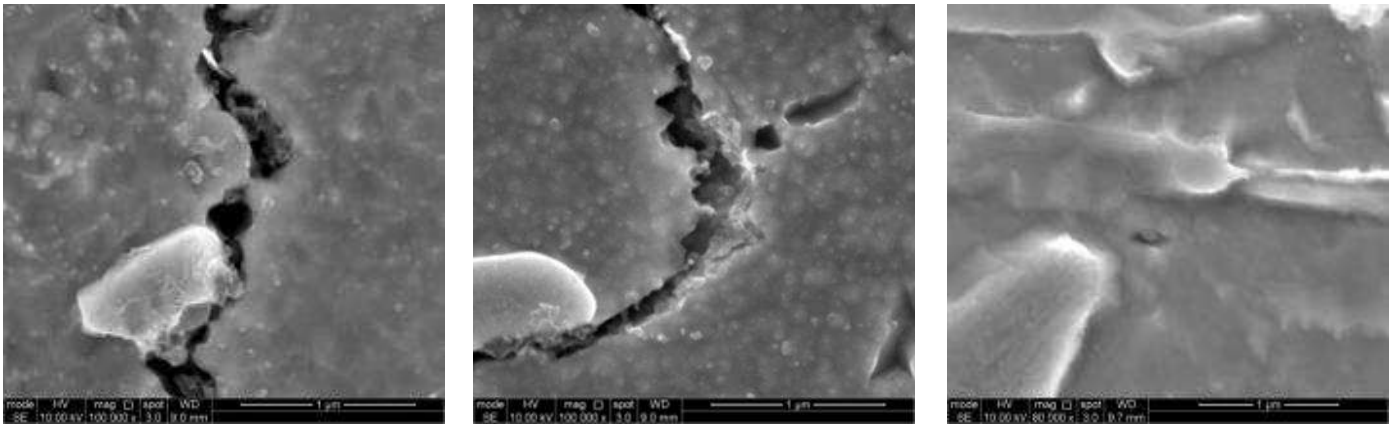

(a) (b) (c)

Fig. 7 Sub-micron void formation within the ferrite phase right before the final failure due to decohesion of carbide particles or Mn-S inclusions

3.3 Local strain measurement

The local deformation of the microstructure has also been quantified using DIC for the micrographs of the deformed specimen taken at low and high magnifications. The technique that was developed to measure strain distributions within the deformed microstructure as well as the local strain values at the onset of damage for the identified mechanisms is explained elsewhere [9, 20]. The distribution of the strain component along the loading direction that is in the vertical direction of the image is shown in Fig. 8. Local strain values as large as 4.5 have been measured within the ferrite phase, although no localized strain bands have been detected within the microstructure, in contrast to the strain map reported for DP1000 in [9]. The strain maps of Fig. 8 show that the largest local strain values measured are within the ferrite grains and that the deformation is much smaller in the vicinity of martensite islands. Therefore the microstructural deformation is restricted by the presence of the martensite rich regions. The images taken at the higher magnification have been analysed to resolve the deformation within the martensite phase. Fig. 9 shows the measured strain distribution within the selected region of microstructure in Fig. 3c close to the yield point (Fig. 9a) and just before the final fracture (Fig. 9b). Although the strain maps show a good correlation has been obtained in most of the analysed area, there are some small regions in the ferrite grains that correlation has not been made due to the lack adequate random pattern within the ferrite phase.

The martensite boundaries are highlighted for better visualization of the deformation within the islands. The maps clearly show that the martensite phase is plastically deformable with a heterogeneous strain distribution within the phase. Fig.9a indicates that the large local strain values of about 20% are measured close to the identified damage initiation sites (shown by the arrows). The local strain values for the identified damage

mechanisms have also been determined from the obtained strain maps. It is found that crack initiation occurs at a local strain value of 17% and 5% for the mechanism shown in Figs. 4a and 4b, respectively. The fracture strain of martensite therefore varies significantly as it is dependent upon several factors including the size and geometry of the martensite grains together with the local stress state around the phase.

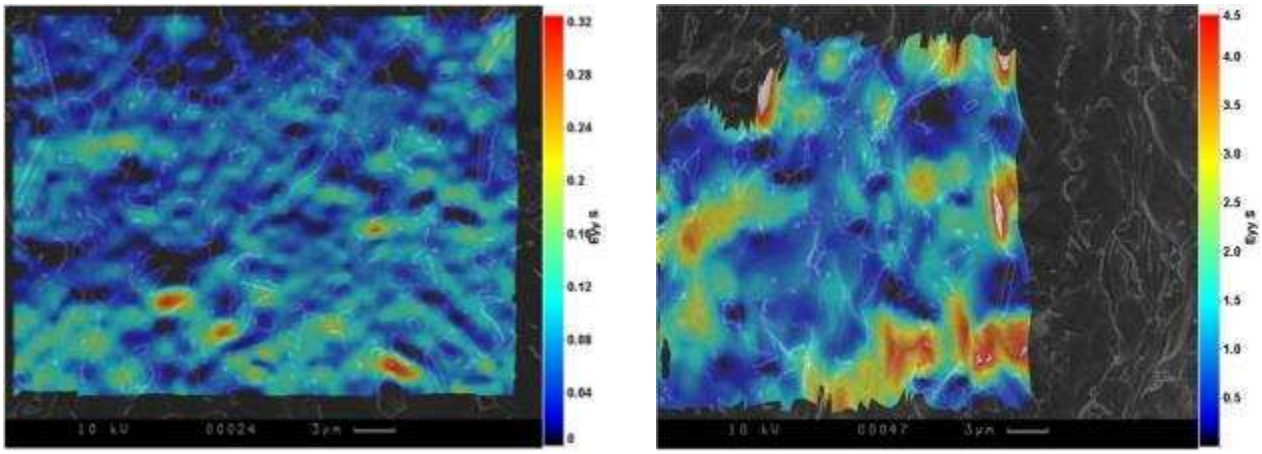

(a) (b)

Fig. 8 Local strain distributions at the applied strain of (a) 14 % and (b) 88% for the micrographs shown in Fig. 3a that shows the deformation evolution in the microstructure

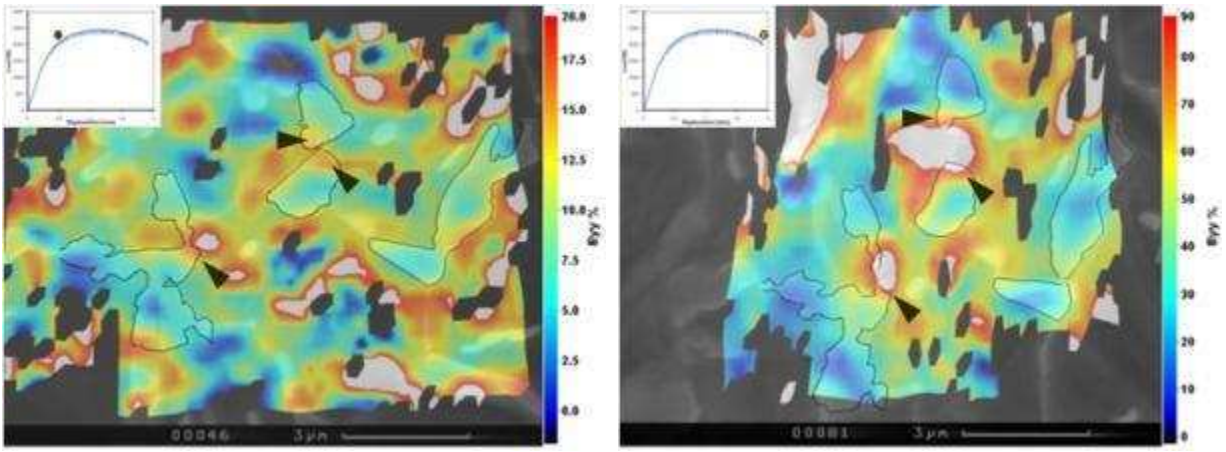

(a) (b)

Fig. 9 Local strain distribution in the martensite islands for the microstructure of Fig. 3c obtained (a) close to the yield point and (b) before the final fracture of the specimen that shows the strain gradient within the highlighted martensite islands together with the local strain values close to the damage initiation sites shown by arrows

3.4 Damage evolution

Fig. 10a shows the recorded load-post uniform elongation for the tensile specimens with the G2 gauge geometry. The modified gauge geometry results in a slower damage evolution rate that provides an opportunity to investigate final stages of damage propagation within the material. The solid line in Fig. 10a corresponds to the broken specimen while the curves with broken lines represent the tests interrupted before final fracture.

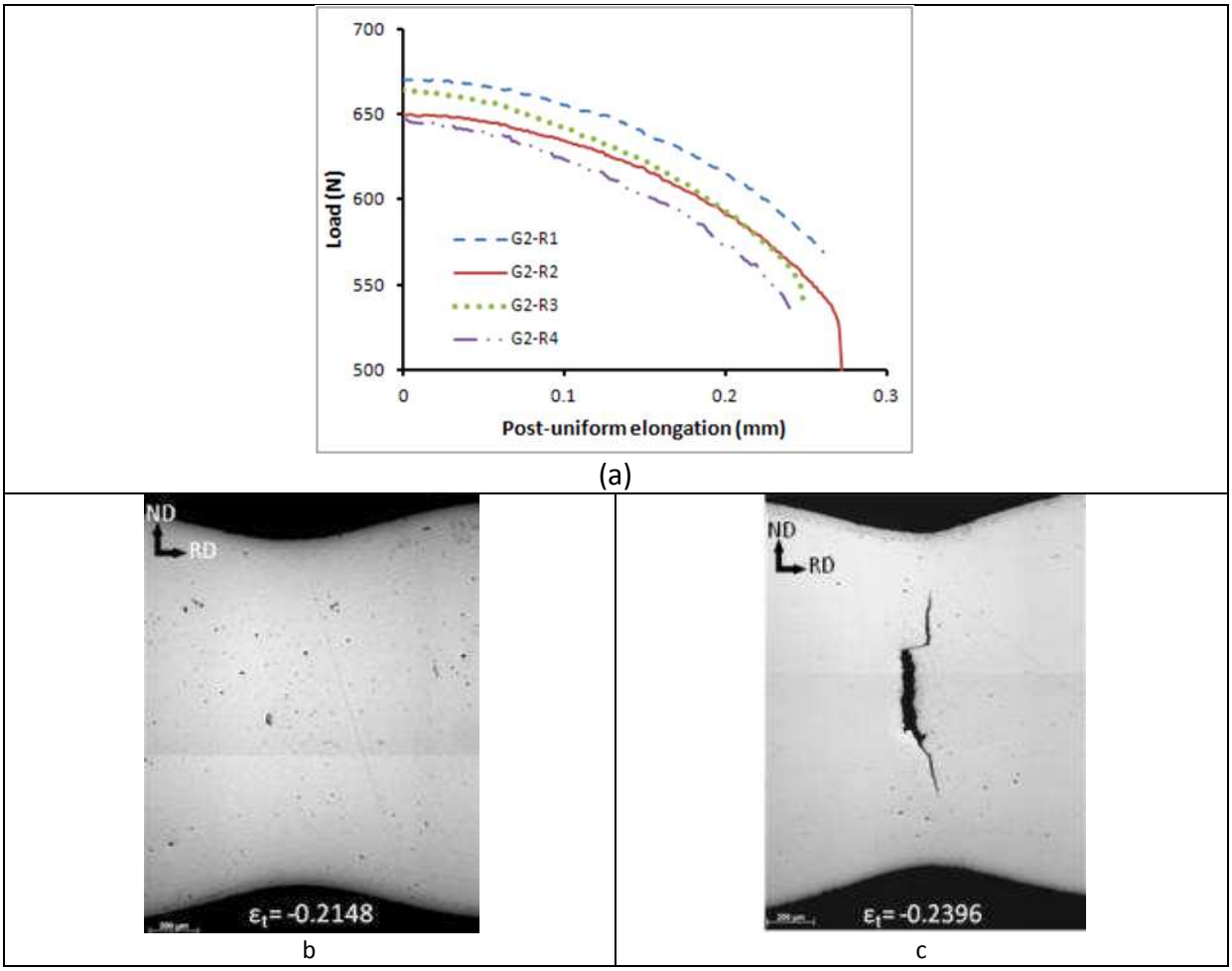

Fig. 10 (a) Load-post uniform elongation curves for samples with G2 gauge geometry loaded in the rolling direction and Optical micrographs of the mid-width plane of (b) G2-R1 and (c) G2-R3 tensile specimens for the tests stopped before final fracture

Optical micrographs of samples R1 and R3 are shown in Fig. 10b,c together with the through thickness strain values corresponding to each sample. The images show that final fracture starts at the centre of the neck where the voids volume fraction is greatest. The small strain increment between the two steps (R1 and R3) indicates that the damage propagation occurs due to a very rapid voids coalescence followed by crack propagation near centre of the neck that results in final fracture. The material fails perpendicular to the loading direction at the stage shown in Fig. 10b,c with an untypical step that shows the competition between localised variations in microstructural damage intensity with the necking geometry. The position of the final crack had to adjust to plane of greatest stress where the cross-section area was minimal at the neck.

Figure 11 shows how the voids are connected at the mid-width plane of the specimen during the damage evolution. Void coalescence due to the interconnection of growing voids initiated at close proximity from each other (Fig. 11a) is a well-known mechanism of ductile failure. However as the voids initiate apart from each other, damage evolution occurs through micro-crack initiation and its propagation through the ferrite phase between the growing voids (Fig11b). The crack propagation path is affected by the microstructural constituents ahead of the crack tip. Fig. 11c shows that the crack has been deflected to

avoid martensite islands located in its path. However, when there is no alternative route for crack propagation, the crack passes through the martensite and can fracture the islands (Fig.12).

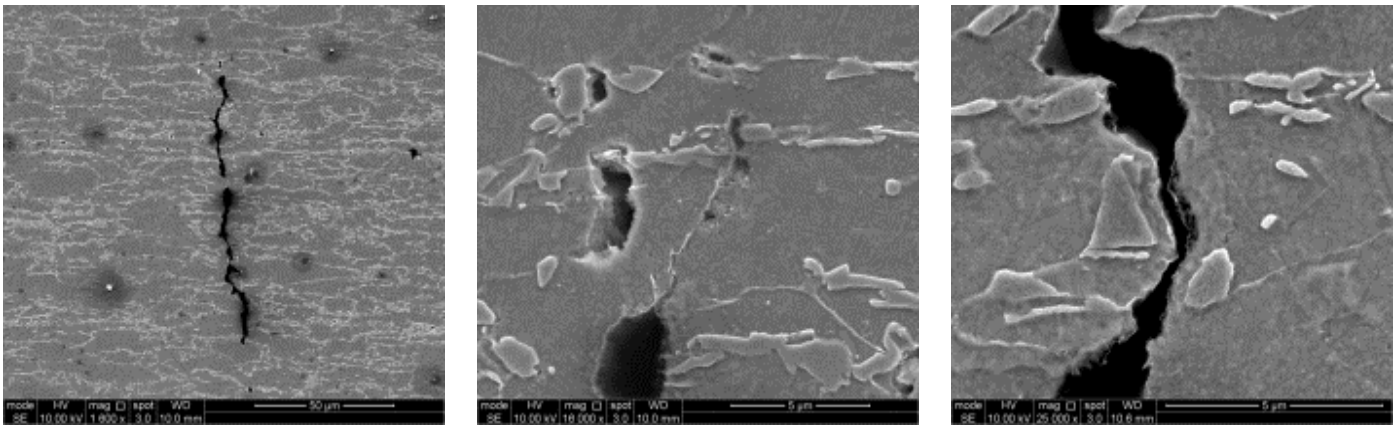

(a) (b) (c)

Fig. 11 High resolution micrographs at the mid-width plane of specimens showing different damage evolution mechanisms including interconnection of voids by crack propagation between the adjacent damage sites

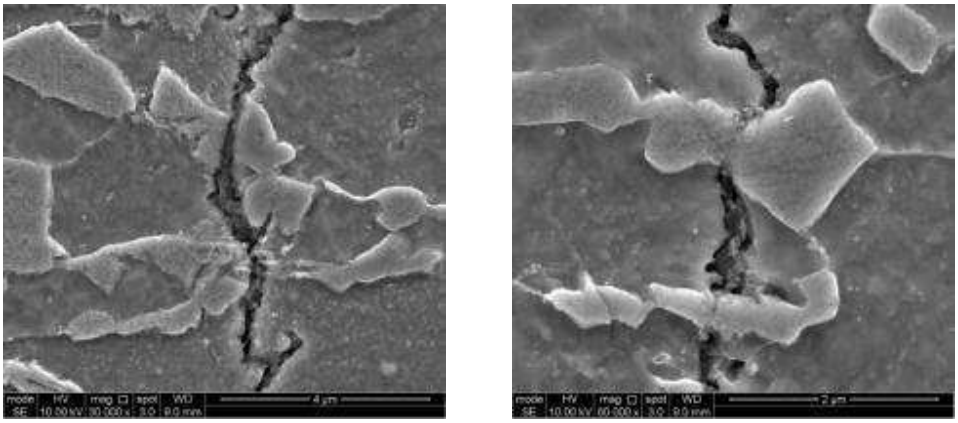

(a) (b)

Fig. 12 Facture of martensite islands due to crack propagation during damage evolution

4 Discussion

4.1 Mechanisms of local deformation

In-situ micro-tensile tests together with the DIC technique have been used to quantify the local deformation and damage mechanisms in a commercial DP600 steel. Based on Fig. 3 and the strain maps shown in Fig. 8, local deformation starts within the largest ferrite grains at the early stages of deformation, which has also been observed in other DP steel grades [9, 15]. This might be related to the lower GND density at the centre of larger ferrite grains compared with the boundary regions [21]. The lower dislocation density in the grains interior is related to the fact that centre of the grains are less affected by the martensitic phase transformation, therefore the internal elastic stresses are close to the elastic limit of the undeformed ferrite[22]. Consequently, plastic yielding occurs at much smaller applied strain in the grain interior and generates a considerable misorientation gradient in the ferrite phase [21] with much higher lattice curvature close to the F-M interface[23].

The mechanisms of deformation in ferrite are reported to be closely related to the size and the orientation of the grains as reported in [21]. The in-grain orientation gradient is higher for the smaller ferrite grains surrounded by martensite islands [21]. Additionally, the induced plastic deformation due to the martensitic volume expansion may induce work-hardening within the ferrite grains [24] and thus, increase the dislocation densities adjacent to the F-M interface. Consequently, higher local stresses are required to plastically deform smaller ferrite grains. This may occur after severe plastic deformation within the neighbouring larger grains (F2 in Fig. 4). However, in the larger grains deformation is localized in the form of slip bands at the early stages of deformation (F1 in Fig. 3) and sub-grain structures are formed [3, 23] , as shown in Fig. 13. The dislocation density is increased in these substructures and this may facilitate damage initiation and crack propagation in a heavily deformed ferrite grain (Fig. 13).

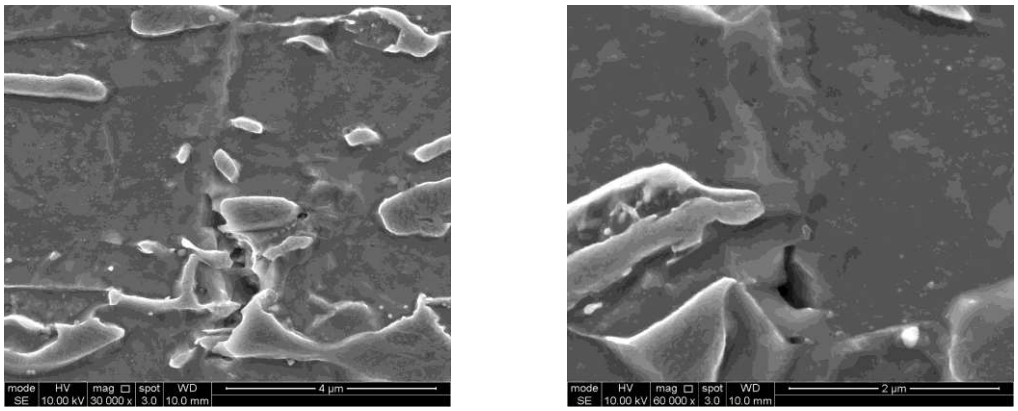

(a) (b)

Fig. 13 Damage initiation and crack propagation along the sub-grain structures in the ferrite phase due to an excessive plastic deformation

4.2 Plastic deformation of martensite

It is shown that martensite is clearly a deformable phase within the microstructure of DP-steels (Fig.3, 4 and 9), even when the macroscopic stress applied is tensile. The strain map of Fig. 9b shows that a maximum local strain value of about 80% is measured within the islands close to the phase boundaries. However it is worth noting that an average error of about 16% may exist in the measured strain values in the used DIC technique and SEM micrographs as reported elsewhere [20].

Local deformation of the martensite phase has also been reported for other DP steel grades [3, 9, 16]. The measured local strain values are dependent not only on the carbon content, the volume fraction of the martensite phase, the microstructural morphology of the material, but also the selected parameters to calculate strain values using the DIC algorithms[20]. It has been reported that the carbon content of austenite increases by reducing the grain size [25]. Consequently, larger martensite areas are expected to have lower hardness and therefore, are more deformable than smaller islands.

By considering DP steels as a composite material, the lower strength difference between ferrite and larger martensite islands promotes plastic deformation of the latter [26]. This is however only valid for a uniform distribution of martensite islands with a relatively similar

configuration like that observed for regions 2 and 6 in Fig. 3a. However, the smaller martensite islands may undergo larger plastic deformation due to the specific microstructural arrangement around the islands. Fig. 14 shows the lower magnification micrograph of the selected region of Fig. 3c. Here, the smaller islands (e.g. A) are located at the direct vicinity of two small ferrite grains, F2 and F3, while the larger martensite island (B) is enclosed by much larger ferrite grains (F4 and F5). The ferrite grains F2 and F3 are surrounded by several martensite islands and therefore, the volume expansion of the martensite islands during phase transformation may generate a local stress field inside the grains that plastically deforms the whole grain. Due to the subsequent work hardening, the local yield strength of ferrite increases to a value close to that of the neighbouring martensite islands. However, for the larger ferrite grains F4 and F5, the martensitic volume expansion affects a narrow rim along the phase boundaries leading to a much larger yield strength difference between the ferrite grains and martensite islands. Accordingly, at an applied elongation, the local stress field is more uniformly partitioned between the two phases in the ferrite-martensite cluster containing smaller ferrite grains [3] and local stresses are more rapidly transferred to the martensite phase [27]. As a result the martensite island denoted A, might be subjected to a larger local stress field than island B that has a better strain compatibility with the ferrite grains around and that results in a larger plastic deformation in the island (Fig. 9b). The grain size and the martensite volume fraction in the steel are other important factors affecting the global and local ductility of the material and are reported elsewhere [3].

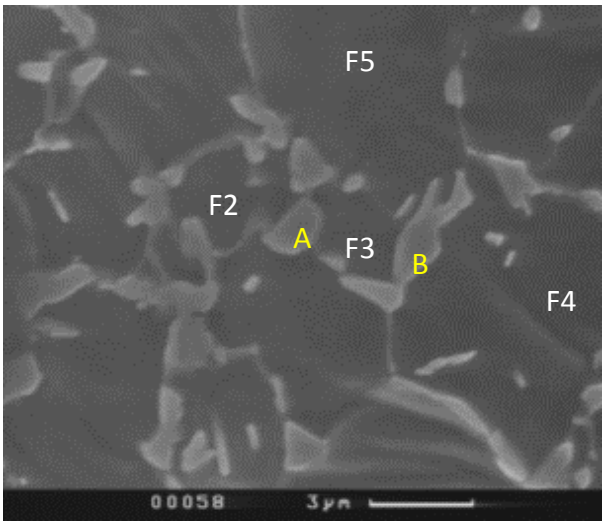

Fig. 14 lower magnification micrograph of Fig. 4 that shows the effect of microstructural configuration on the local deformation mechanism

4.2.1 Non-uniform strain distribution

While martensite is plastically deformable, the strain maps in Fig. 9 show that there is a heterogeneous strain distribution across the islands with larger strain values close to the phase boundaries than the centre of the islands. This variation of strain values across the martensite islands are plotted in Fig. 15 for the martensite islands A and B (Fig. 14). The plots show that the local deformation is not uniform along the specified line shown with blue colour. Fig. 15a and b show a higher strain value on the left-hand edge of the martensite islands while the local strain value at the right-hand side of the island is lower compared to the centre. The strain values at each individual step in the plots correspond to

the local deformation of subsets used for DIC analysis. Therefore the flat sections of the plots show the strain values within each individual subset across the predefined line. According to the strain maps of Fig. 9, the deformation gradient within the martensite phase is dependent upon the geometry and size of the individual islands. The local strain values at the F-M interface cannot be independently quantified due to the fact that the displacements of pixels located at the either side of the interface are considered to determine the total strain of a selected subset size that covers the interfacial regions.

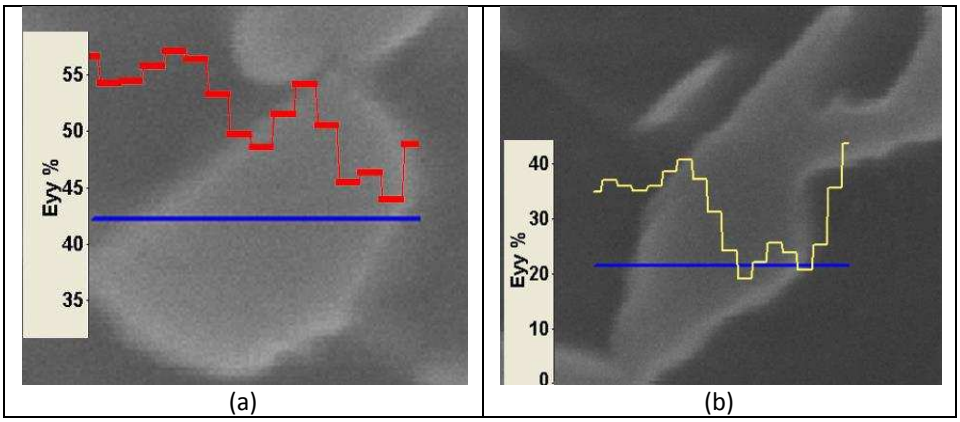

Fig. 15 local strain distribution across the martensite island (a) A and (b) B shown in Figure 20 along the specified line (blue line)

The heterogeneity of plastic deformation in the martensite phase can however be explained by the fact that the dislocations density is not distributed evenly in the islands [21]. The larger martensite islands experience more deformation heterogeneity due to the higher variations in carbon content[24], a non-uniform distribution of alloying elements (e.g. Mn) [28, 29] The gradient of carbon content between the interface and the centre of the martensite island can affect the hardness and dislocation configurations and consequently, the formability of the grains in different locations [24].

4.3 Damage initiation due to martensite failure

Void formation due to the failure of martensite islands is one of the identified damage initiation mechanisms for DP steels [3, 11, 30]. This may occur as a result of the separation of prior austenite grain boundaries (Fig. 3) and/or crack initiation and propagation through the martensite islands. The segregation of alloying elements such as residual phosphor often occurs at the prior austenite grain boundaries, which increases their brittleness [3]. Additionally the plastic incompatibility between adjacent martensite islands would make these boundaries the likely failure initiation sites. On the other hand, Szewczyk and Gurland [31] reported that the plastic incompatibility increases the average applied stress at the hard phase above the mean stress value in the dual phase alloys. They showed that the local uniaxial stress in martensite can be 3 times larger than the ferrite stress. Therefore at an applied large plastic strain, the martensite phase is subjected to a relatively large local stress, close its yield strength, that will result in a local plastic deformation. Additionally the carbon is heterogeneously distributed in the martensite islands[24], the boundary regions of the martensite islands are prone to failure in a form of crack initiation due to higher carbon concentration and the reduced ductility compared to the interior of the islands. This may explain the fact that cracks formation are mostly observed at the boundary region of the martensite islands as shown in Fig. 4.

It is worth noting that since no F-M decohesion has been observed in the studied material, one can conclude that the F-M interface is very coherent with a shear strength much higher than the tensile strength of the martensite phase.

Martensite island failure occurs at different local strain values depending on the mode of deformation for each island. The magnitude of the local strain at fracture is related to the local stress field around the deforming martensite islands as a local strain value of 17% was measured for the crack initiation due to tensile deformation shown in Fig. 4a while the bending crack (Fig. 4b) was initiated at a much smaller local strain value of about 7%. The measured critical strain values are higher than those reported by Avramovic-cingara et al [11] for damage initiation by martensite cracking in a DP600 steel, which were 3% for martensite cracking and 9% for the failure at ferrite-martensite interface. This could be due to the different microstructural morphology in the tested materials. Additionally, the selected DIC parameters used for strain calculation play an important role in the calculated strain values [20] and the selected grid size for strain measurement in [11] might be considerably larger than the one used in the present study that would result in a large variation in the measured strain values.

4.4 Damage mechanisms at F-M interface

The higher hardness of the interfacial regions of the ferrite grains [24] together with a higher concentration of alloying elements, as previously explained, may produce an effective barrier for the dislocation movement. The higher dislocation density in the F-M and F-F boundary [21, 22, 24] makes it more difficult for dislocations transmission through the boundaries[24] during plastic deformation and therefore, increases further the dislocation density at these narrow bands around the martensite islands. As a result, strain heterogeneity increases within the ferrite grains and higher levels of deformation may occur close to the interfacial regions in smaller ferrite grains. The plastic deformation is localised in these regions by further applied elongation until failure occurs in the form of submicron voids formation close to the F-M interface (Fig. 5). The voids are elongated by further deformation localisation leading to micro-cracks followed by their propagation along the boundary, as shown in Fig. 5c. A similar explanation can apply to the void initiation close to both the F-F interface and triple junctions of the grains. The local hardness [24] and dislocation density [21] are higher in these regions compared to the interior of the grains and therefore facilitate voids formation during local plastic deformation. Therefore failure of the ferrite phase is the main mechanism involved in the formation of such elongated voids rather than grain boundary separation as stated in [30]. This type of elongated voids are also reported by Avarmovic-cingara et al [7] for a commercial DP steel.

4.5 Damage evolution and final fracture

Special gauge geometry was designed to study the final stages of damage evolution and fracture propagation during the tensile experiments (Fig. 1b). The rate of damage and fracture propagation in the standard tensile specimen geometry was so fast that it was not possible to capture intermediate stages of damage evolution in the studied material. This could be related to the stress state within the material and the effect of stress triaxiality. Consequently, the gauge geometry was modified in such a way to reduce the damage propagation rate at the centre of the neck. The modified specimen geometry made it possible to capture the intermediate stages of damage propagation and investigate the effect of microstructural constituents on the final stages of deformation. Fig. 10 shows that

the final failure occurs after voids accumulation at the central region of the neck. The initial failure may occur due to either the coalescence of several growing voids formed at close vicinity or by crack initiation and propagation through ferrite linking the voids formed within a large ferrite grain, Fig. 11. Cracks propagated by following the path of least resistance, which was largely within the ferrite matrix as opposed to the martensite islands. This includes the regions away from the phase boundaries as shown in Fig. 11d. As explained earlier, the area close to the F-M interface has higher hardness [24] and larger dislocation density[21] compared with the grain interior. Therefore, the cracks propagation through the area away from the phase boundaries requires lower fracture energy. Additionally, fracture of martensite islands are also observed in the area close to the edge of the specimen (Fig.12) towards the end of the test, as the stress triaxiality increases within the region of the neck. It is shown that the crack has directly passed through the martensite islands with a sharp crack edge. In contrast to the voids initiated close to the F-M boundaries, those are observed within the ferrite grains are formed due to the decohesion of Mn-S inclusion and possibly very fine carbide particles dispersed in the ferrite grains. It has been reported[21] that a large local deformation gradient is required for the decohesion of fine carbide particles from the ferrite matrix. This may happen towards the end of the test where ferrite grains undergo a large local plastic deformation; hence, providing the required condition for the submicron voids formation.

5 Conclusions

Local deformation and damage initiation mechanisms in a commercial DP600 steel have been studied in the present research. Digital Image Correlation has been used to quantify local deformation within the microstructural constituents using successive micrographs taken during in-situ tensile tests. A heterogeneous plastic deformation has been observed in the microstructure with the deformation being localized within the large ferrite grains. It is found that martensite is plastically deformable and a non-uniform local strain distribution has been measured within the phase with local strain values as large as 80% close to the phase boundaries. The martensite failure occurs due to crack initiation from the interfacial regions followed by its propagation towards the interior of the islands. The cracks are formed as a result of plastic deformation of the martensite islands with a total elongation as large as 13.5 % or as a result of deformation localisation in the form of slip bands inside the large martensite islands followed by shear fracture. A new gauge geometry has been proposed to study the damage evolution mechanisms in the material. It is shown that the damage evolution occurs due to both void coalescence and micro-crack formation within the microstructure. It is found that sub-micron voids are formed inside the large ferrite grains as a result of decohesion of sub-micron carbide particles and Mn-S inclusions from the ferrite matrix.

6 Acknowledgement

This research was carried out under project number M41.2.10398 in the framework of the Research Program of the Materials innovation institute- M2i (www.m2i.nl). The authors would also like to thank Tata Steel R&D, IJmuiden in the Netherlands for providing the material of this study.

7 References

[1] Koo JY, Thomas G. Design of duplex low carbon steels for improved strength: weight applications. In: Davenport AT, editor. Formable HSLA and dual-phase steels. NewYork: AIME, 1977. p.40.

[2] Sarwar M, Priestner R. Journal of Materials Science 1996;31:2091.

[3] Calcagnotto M, Yoshitaka A, Ponge D, Raabe D. Acta Materialia 2011;59:658.

[4] Gerbase J, Embury JD, Hobbs RM. The mechanical behaviour of some dual phase steels with emphasis on the initial work hardening rate. In: Kot RA, Morris JW, editors. Structures and properties of dual phase steels. NewYork: AIME, 1979. p.118.

[5] Erdogan M. Journal of Materials Science 2002;37:3623.

[6] Steinbrunner DL, Matlock DK, Krauss G. Metallurgical Transactions A 1988;19:1821.

[7] Avramovic-Cingara G, Saleh CAR, Jain MK, Wilkinson DS. Metallurgical and Materials Transactions A 2009;40A:3117.

[8] Kang J, Jain M, Wilkinson DS, Embury JD. Journal of Strain Analysis 2005;4:559.

[9] Ghadbeigi H, Pinna C, Celotto S, Yates JR. Materials Science and Engineering A 2010;527:5026.

[10] Erdogan M, Tekeli S. Materials and Design 2002;23:597.

[11] Avramovic-Cingara G, Ososkov Y, Jain MK, Wilkinson DS. Materials Science and Engineering A 2009;516:7.

[12] Kadkhodapour J, Butz A, Ziaei Rad S, Schmauder S. International Journal of Plasticity 2011;27:1103.

[13] Shen HP, Lei TC, Liu JZ. Materials Science and Technology 1986;2:25.

[14] Tatschl A, Kolednik O. Materials Science and Engineering A 2003;339:265.

[15] Ososkov Y, Wilkinson DS, Jain M, Simpson T. International Journal of Materials Research 2007;98:664.

[16] Kang J, Ososkov Y, Embury JD, Wilkinson DS. Scripta Materialia 2007;56:999.

[17] Jin H, Lu W-Y, Korellis J. Journal of Strain Analysis for Engineering Design 2008;43:719.

[18] Calcagnotto M, Ponge D, Raabe D. Materials Science and Engineering A 2010;527:7832.

[19] Uggowitzer P, Stuwe HP. Materials Science and Engineering 1982;55:181.

[20] Ghadbeigi H, Pinna C, Celotto S. Experimental Mechanics 2012;DOI:10.1007/s11340-012-9612-6.

[21] Calcagnotto M, Ponge D, Demir E, Raabe D. Materials Science and Engineering A 2010;527:2738.

[22] Sarosiek AM, Owen WS. Materials Science and Engineering 1984;66:13.

[23] Dillien S, Seefledt M, Allian S, Bouaziz O, Van Houtte P. Materials Science and Engineering A 2010;527:947.

[24] Tsipouridis P, Koll L, Krempaszky C, Werner E. International Journal of Materials Research 2011;102:674.

[25] Moyer JM, Ansell GS. Metallurgical Transaction A 1975;6:579.

[26] Lian J, Jiang Z, Liu J. Materials Science and Engineering A 1991;147:55.

[27] Jiang Z, Guan Z, Lian J. Materials Science and Engineering A 1995;190:55.

[28] Navara E, Bengtsson B, Easterling KE. Materials Science and Technology 1986;2:1196.

[29] Sun S, Pugh M. Materials Science and Engineering A 2000;276:167.

[30] Kadkhodapour J, Butz A, Ziaei Rad S. Acta Materialia 2011;59:2575.

[31] Szewczyk F, Gurland J. Metallurgical and Materials Transactions A 1982;13:1821.